Two-Dimensional Analysis of Integrated Three-Pulse Photon Echo Signals of Nile Blue Doped in PMMA

Yutaka Nagasawa,* Kazushige Seike, Takayuki Muromoto, and Tadashi Okada

Department of Chemistry, Graduate School of Engineering Science, and Research Center for Materials Science at Extreme Conditions, Osaka University, Toyonaka, Osaka 560-8531, Japan

Received: September 17, 2002; In Final Form: January 14, 2003

The integrated three-pulse photon echo signal of Nile blue doped in poly(methyl methacrylate) (PMMA) was measured two-dimensionally by varying the first coherence period and the subsequent population period. The electronic dephasing time was in the femtosecond time range even at low temperatures, whereas rephasing and echo formation were still possible even when the population period was extended to >100 ps. Oscillation was present in the echo signal even when population period was extended to longer values than the dephasing time of the vibrational coherence. Echo peak shift measurement indicated a presence of small spectral diffusion in the picosecond time range. A computer simulation was carried out from a model spectral density. The phonon mode of PMMA was represented by a Brownian oscillator centered at ∼116 cm^{-1}, and it reproduced the temperature dependence of the echo signal surprisingly well.

1. Introduction

Solvation dynamics have been studied extensively because of their importance in solution-phase chemical reactions, especially for the electron-transfer reactions.[1−10] Some electron transfer reactions that do not occur in a vacuum or nonpolar solvents can take place in polar solvents. It is considered that the energy relaxation caused by the solvation is the driving force of the reaction, and the relation between the reaction rate and the solvation dynamics have been studied in detail. Solvation dynamics are usually studied using a nonreactive solute−solvent system, in which the solute molecule changes its value of electric dipole moment on photoexcitation. When the solute molecule is excited by a short laser pulse, the dipole moment instantaneously changes its value and/or direction. The solvent molecules, which were oriented around the solute molecule in a manner to minimize the free energy of the ground state, subsequently reorganize to a new solvation structure suitable for the charge distribution of the excited molecule. This solvation process on the excited state can be studied by the measurement of dynamic Stokes shift by means of femtosecond fluorescence up-conversion technique.[3,4,7] When the laser line-width is shorter than the inhomogeneous line-width of the absorption spectrum of the solute molecule, a hole-burning technique can be employed to measure the time scale of the solvation process in the ground state.[11,12] Recently, advanced photon echo techniques have been applied to the study of solvation dynamics.[13−20]

Solvation process can be roughly separated into two components, i.e., the inertial component which appears on the time scale of ∼200 fs or shorter and the diffusive component which appears in the picosecond time regime.[1,3,5,6,9] The inertial component is caused by the small angle free rotation of a few solvent molecules within the first solvation shell, whereas the diffusive component is caused by the diffusive rotation and translation of the bulk solvent. The inertial component is often approximated by a Gaussian function because the time differential at time origin has to be zero. [8] The diffusive component is usually expressed by multiexponential or stretched-exponential function, which may be ascribed to the hierarchy structure of the solvation shell.

Optical dephasing measurements such as photon echo and hole-burning were originally used to study line broadening mechanisms in low-temperature solids.[21,22] At temperatures lower than liquefied helium, the major homogeneous line broadening mechanism of chromophores in glassy hosts is the phonon assisted tunneling, and it is often described by a two level system (TLS) model.[23,24] The TLS model postulates that chromophores can reside in not just one but two potential minima of the local structure of the glass. Transitions from one well to the other represent changes in the local structure. The TLS model states that there is a very broad distribution of double well energy differences and tunneling parameters, and tunneling among these TLSs gives rise to the homogeneous width of the zero-phonon line. The hole burned in the absorption spectrum of a chromophore in low temperature glass is often clearly separated into the zero-phonon line and phonon-side band. When the temperature is raised, the phonon modes will be thermally excited and the hole becomes broader and featureless like the ones observed in room-temperature liquids.

Because the glass and liquid are both disordered condensed phases, it is interesting to compare and examine the theories and methods developed in both fields. Like the solvation process in liquids, the line broadening dynamics in low-temperature glass can be also separated into fast and slow processes.[21,22] The fast process is the optical dephasing process in the picosecond time region which can be observed by photon echo spectroscopy. The slower process is called the "spectral diffusion" and occurs on time scales of microsecond, millisecond, and beyond. The major physical difference between the liquid and the glass is the existence of static inhomogeneity in the glass. In liquids, all of the relaxation processes take place on a finite time scale. Therefore, any nonequilibrium state will eventually reach thermal equilibrium. This property of a liquid is called "ergodicity". On the other hand, some processes in glasses take an infinitely long time to relax, and the thermal equilibrium will

* To whom correspondence should be addressed.

10.1021/jp027012m CCC: $25.00
Published on Web 03/14/2003

never be achieved. The spectroscopy which clearly showed this difference between glass and liquid was the three pulse photon echo peak shift measurement.

The three-pulse photon echo peak shift (3PEPS) measurement is a modified photon echo spectroscopy widely used to obtain time scales of solvation and protein dynamics.[13,15−17,25−48] The three pulse photon echo technique is basically a three-dimensional spectroscopy because there are three time intervals to consider. The first time interval is called the coherence period, τ, where the electronic coherence is formed by the first ultrashort laser pulse and the optical dephasing takes place. The second time interval between the second and the third pulse is called the population period, T, where the optical phase at the arrival time of the second pulse is recorded in the medium as a spatial-spectral hologram. During T, optical dephasing still proceeds, however, the recorded phase information remains as long as the spatial-spectral hologram is not destroyed. The third time interval, which begins after the last pulse, is called the second coherence period, τ', where rephasing and echo formation take place. In other words, the third pulse reads out the phase information recorded in the medium. In the 3PEPS measurement, τ and T are controlled and the signal integrated over τ' is measured. Two photon echo signals appearing in the phase-matching direction of $-\mathbf{k}_1 + \mathbf{k}_2 + \mathbf{k}_3$ and $\mathbf{k}_1 - \mathbf{k}_2 + \mathbf{k}_3$ are simultaneously measured. The echo intensities are measured as a function of τ with a fixed value of T. The shift of the echo intensity peak from $\tau = 0$ is defined as the echo peak shift. The peak shift measurement is repeated after each stepwise increment of T. The plot of the echo peak shift as a function of T is constructed as the 3PEPS signal. The peak shift reflects the rephasing and echo formation capability of the medium. When T is elongated and the solvation process proceeds, the spatial-spectral hologram will be destroyed and the peak shift decreases.

The echo peak shift was first measured by Ippen and co-workers for a dye-doped polymer glass as a function of temperature. [49,50] The echo peak shift increased from 0 to 30 fs when temperature was decreased from 290 to 15 K for a dye, cresyl violet, doped in PMMA. They ascribed the increase of the peak shift to the transition from homogeneous to inhomogeneous broadening of the absorption spectrum. The peak shift measurement was first applied to room-temperature liquid by Joo and Albrecht. [51] They observed a decrease of the peak shift as a function of T for an oxazine dye in ethylene glycol. The 3PEPS measurement has been extensively applied to the study of solvation dynamics by Fleming,[13,15,16,25−33] Wiersma,[17,34,35] and their co-workers. The difference between the polymer glass and liquid was first measured by Nagasawa et al.[52−54] They observed decay of the peak shift in the picosecond time domain caused by the diffusive solvation process in room-temperature ethanol, whereas the peak shift remained constant in polymer glass during the same time regime. The 3PEPS measurement has been applied to the studies of nondipolar solvation,[28,55] phospholipid/water interfaces,[56] protein-matrix dynamics,[36−39] energy transfer in bacterial light-harvesting complex,[40−47] electron transfer in photosynthetic reaction center,[48] and in electron donating solvent.[57]

Despite all of the valuable information obtained by the 3PEPS measurement, this method only monitors the peak position of the echo signal and ignores other features such as shape and intensity. This is not a big problem in room temperature liquid, where the electronic dephasing is ultrafast and the echo signal is nearly symmetric. However, in low temperature glassy solids, where the dephasing time is sufficiently longer than the pulse duration and the echo signal becomes asymmetric, monitoring only the echo peak shift may be insufficient for a detailed analysis. It is also known that the echo peak shift depends on excitation wavelength.[25,26,58] To extract all of the information embraced in the signal, the echo intensity should be carefully monitored as a two-dimensional function of τ and T. Here we report two-dimensional measurements of the integrated three pulse photon echo signal by controlling the first and the second time periods, τ and T, and integrating the echo signal over the third period, τ'. The sample we have measured is a Nile blue doped poly(methyl methacrylate) (NB/PMMA) film. NB is a popular organic dye molecule with a large value of extinction coefficient ($\sim$70 000 L mol^{-1} cm^{-1}) and PMMA is also a popular organic polymer glass. Two types of delay control were tested (3PEPS scan and MS scan), and the features of these echo signals are discussed. Temperature dependence of the echo signal was also measured and computer simulations starting from a model spectral density were carried out. The calculated echo signal reproduced the experimental results surprisingly well.

2. Experimental Section

For the echo measurement, a very stable femtosecond cavity-dumped Kerr lens mode-locked Chromium-doped forsterite (Cr: F) laser was developed. The details of the laser were reported elsewhere.[59] The only change in the system is that the laser is no longer pumped by Coherent Compass (diode-pumped Nd: Vanadate laser) but by Spectra Physics Millenia IR, and this exchange resulted in shorter pulse duration. The repetition rate of the cavity-dumping was 100 kHz, and the output was focused into a 4 mm LBO crystal to generate the second harmonic centered at 635 nm. The second harmonic pulse energy was about 4 nJ and it was divided into 3 beams with equal energy by beam splitters. After splitting, the energy of each beam was less than 1 nJ. After passing through the delay line, the three beams were aligned to form an equilateral triangle and focused into the sample as shown in Figure 1a. The autocorrelation traces between all three pulses were measured by a 0.5 mm LBO crystal with the same setup used for the echo experiment. The amount of glass traversed by the beam was adjusted to be equal for autocorrelation and photon echo measurements. The pulse duration was obtained to be 26−28 fs fwhm, assuming a Gaussian pulse. The sample was rotated at 2000 rpm for room-temperature measurement, whereas it was not rotated when the sample was kept in a closed-cycle helium gas cryostat to lower the temperature. The echo signal was detected by a pair of photodiodes (New Focus, model 2031) and lock-in amplifiers (EG&G Instruments, model 5210).

Two types of delay control were carried out for the echo measurement as shown in Figure 1, parts b and c. We call them "3PEPS scan" and "MS scan", respectively, because the pulse delay is controlled in a same manner as the 3PEPS measurement and the mode-suppression (MS) measurement.[19,20,60] For the 3PEPS scan, only the second pulse is scanned for $\tau < 0$ keeping the delay between the first and the third pulse constant. For $\tau > 0$, the second and the third pulse are simultaneously scanned in order to keep T constant. For the MS scan, only the second pulse is scanned in order to keep the delay between the first and the third pulse, T', constant.

The sample was a film of NB/PMMA with a thickness of 100−200 μm with optical density of 1.0−1.5. NB perchlorate was purchased from Exciton and used without further purification. PMMA with an average molecular weight of 120 000 was purchased from Aldrich. NB (3 mg) was dissolved in 40 mL of chloroform and PMMA (2 g) was added into 10 mL of this

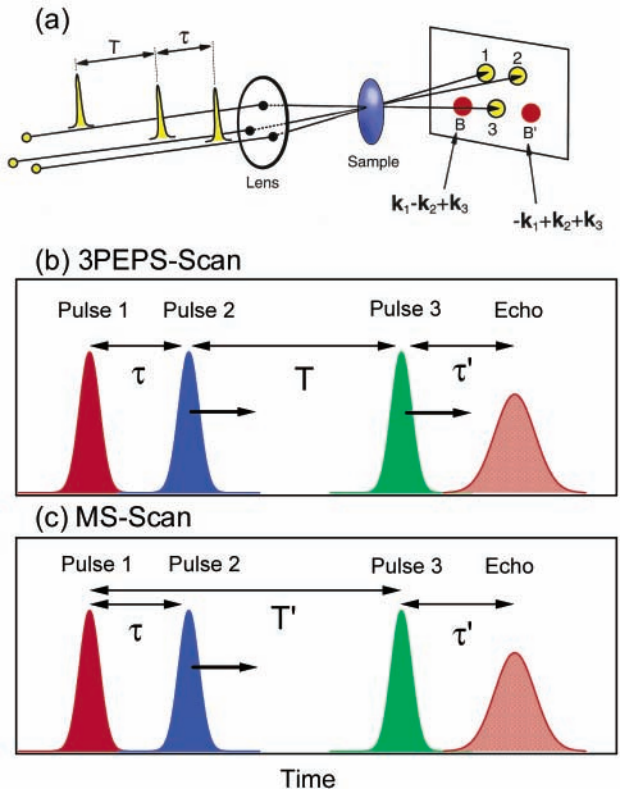

Figure 1. (a) Configuration of the laser pulses and the echo signal. Three laser pulses forming an equilateral triangle were focused into the sample. Interferometric pattern created by pulses 1 and 2 diffracts pulse 3 to the phase-matching directions of $-\mathbf{k}_1 + \mathbf{k}_2 + \mathbf{k}_3$ and $\mathbf{k}_1 - \mathbf{k}_2 + \mathbf{k}_3$. (b) Time-ordering of the pulses for 3PEPS-scan. For $\tau < 0$ fs, pulse 2 is scanned alone, whereas for $\tau > 0$ fs, pulses 2 and 3 are scanned simultaneously. (c) Time-ordering of the pulses for the MS scan. Pulse 2 is always scanned alone.

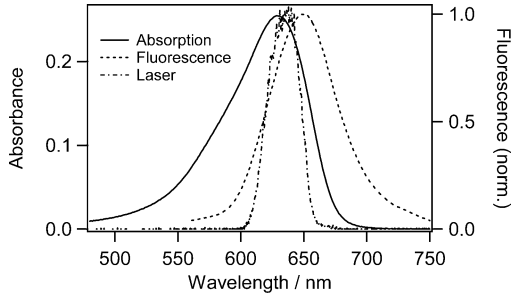

Figure 2. Absorption (solid curve) and fluorescence spectra (dashed curve) of the NB/PMMA film. Laser spectrum centered around 635 nm is also shown (dash-and-dotted curve).

solution. The mixed solution was passed through a 0.2 μm PTFE filter and dropped onto a glass plate. The sample was dried under atmosphere for a day and then kept in a vacuum desiccator for at least a week. The sample film was removed from the glass plate after drying. Absorption and fluorescence spectra of the film were measured by a Hitachi U-3500 spectrophotometer and a 850E fluorescence spectrophotometer, respectively.

3. Experimental Results

Absorption and fluorescence spectra of NB/PMMA at room temperature are shown in Figure 2 and compared with the spectrum of the second harmonic of Cr:F laser. The second harmonic centered around 635 nm excites slightly on the red side of the absorption peak. The Stokes shift between the absorption and fluorescence peak is about 510 cm^{-1}. The photon

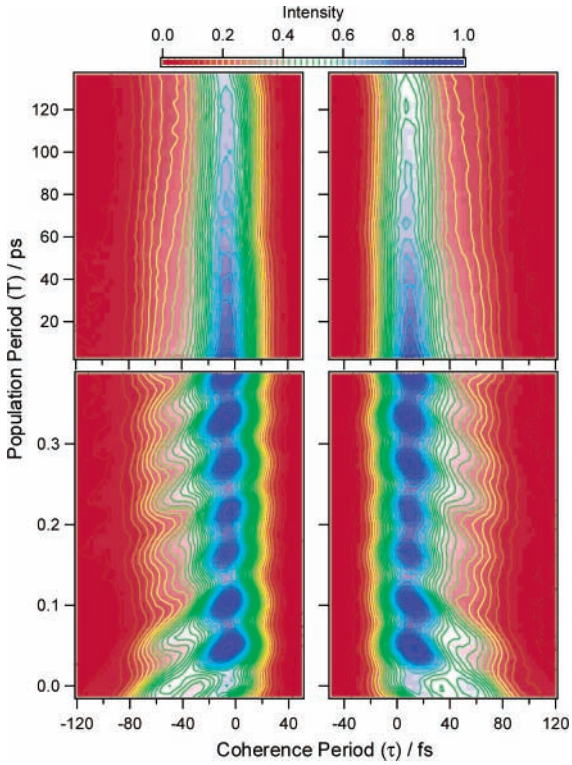

Figure 3. Two-dimensional plot of 3PEPS-scanned photon echo signals of NB/PMMA at 30 K. The right side corresponds to the signal generated at the phase-matching condition of $-\mathbf{k}_1 + \mathbf{k}_2 + \mathbf{k}_3$ and the left side corresponds to that of $\mathbf{k}_1 - \mathbf{k}_2 + \mathbf{k}_3$.

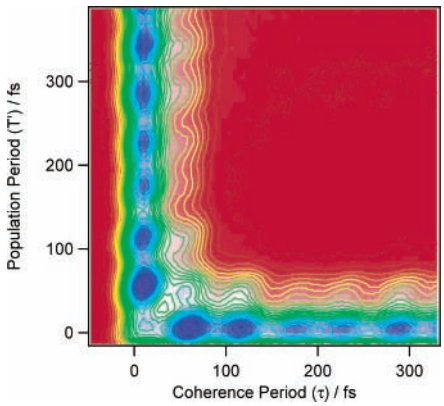

Figure 4. Two-dimensional plot of MS-scanned photon echo signal of NB/PMMA at 30 K generated at the phase-matching direction of $-\mathbf{k}_1 + \mathbf{k}_2 + \mathbf{k}_3$.

echo signals of NB/PMMA at 30 K are plotted in a two-dimensional manner in Figures 3 and 4. Figure 3 represents the 3PEPS-scanned echo signal and Figure 4 represents MS-scanned signal. In both figures, the horizontal and the vertical axes represent the coherence period, τ, and the population period, T, respectively. Therefore, the time scale of optical dephasing is reflected on τ, whereas time scales of the excited-state lifetime and spectral diffusion are reflected on T. In other words, the signal appearing along τ is the conventional echo signal, whereas the signal appearing at $\tau = 0$ along T is the transient grating (TG) signal. It can be easily understood that the electronic dephasing time is extremely short compared to the lifetime of the excited state. The left side of Figure 3 represents the signal appearing in the phase-matching direction of $\mathbf{k}_1 - \mathbf{k}_2 + \mathbf{k}_3$ and the right side is for $-\mathbf{k}_1 + \mathbf{k}_2 + \mathbf{k}_3$. For the 3PEPS scan, the signal generated in the direction of $\mathbf{k}_1 - \mathbf{k}_2 + \mathbf{k}_3$ is the time-

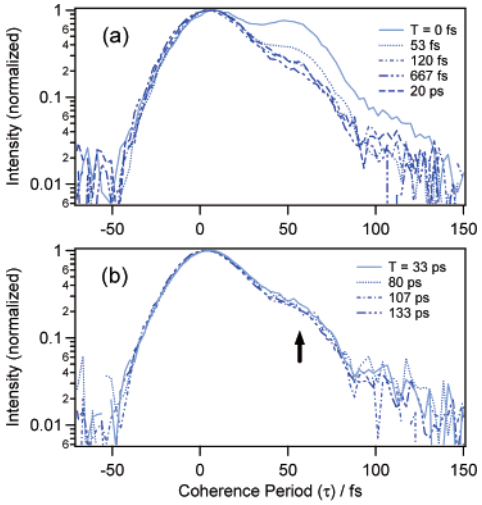

Figure 5. T dependence of the horizontal cross-section of 3PEPS-scanned photon echo signal of NB/PMMA at 30 K generated at the phase-matching condition of $-\mathbf{k}_1 + \mathbf{k}_2 + \mathbf{k}_3$. Note that the bump caused by molecular vibration indicated by the arrow still appears for $T > 30$ ps.

reversal of the signal generated in the direction of $-\mathbf{k}_1 + \mathbf{k}_2 + \mathbf{k}_3$. Therefore, the simultaneous measurement of two signals enables an accurate determination of the position of $\tau = 0$ fs. Only one signal with phase matching direction of $-\mathbf{k}_1 + \mathbf{k}_2 + \mathbf{k}_3$ is shown in Figure 4 for the MS scan. Note that the MS-scanned signal shown in Figure 4 is bent 90° near the time origin and stretched vertically and horizontally toward positive time direction. In this case, the signal extending horizontally along $T' = 0$ fs also depends on excited-state lifetime and spectral diffusion. This effect will be discussed again later. When T is set much longer than the vibrational dephasing time, the MS scan will be equivalent to the 3PEPS scan.

The signals shown in Figures 3 and 4 are modulated mainly by an oscillation with a frequency of 590 cm^{-1}. Note that the ridge caused by the oscillation extends 45° downward in Figure 3, whereas in Figure 4, the ridge extends almost horizontally for the vertical signal along $\tau = 0$ fs and almost vertically for the horizontal signal along $T' = 0$ fs. The same oscillation also appears weakly in the horizontal cross section of the 3PEPS-scanned echo signal shown in Figure 5. The change in the shape of the echo cross-section seen in Figure 5a indicates an existence of fast process, although the cross-section did not change its shape beyond 20 ps. The asymmetric feature of the cross-section shows that rephasing is still capable even when $T > 100$ ps. An interesting point is that the oscillation did not disappear even when T is extended to >100 ps. The arrow in Figure 5b indicates a bump caused by the coherent oscillation.

Peak positions of the echo signal were obtained by fitting the echo signal with double Gaussian function. At room temperature where the echo signals are symmetric, a single Gaussian fitting is acceptable. When the echo signals are not symmetric, however, a more complicated functional form is required. The double Gaussian fitting reduced the amount of peak shift compared to that of the single Gaussian fitting. The obtained 3PEPS signal is shown in Figures 6 and 7 with the results of numerical calculation. Figure 6 shows the short time region of the 3PEPS signal of NB/PMMA. The oscillation with a frequency of about 590 cm^{-1} is apparent at 30 K, whereas it gets weaker at 295 K. The longer part of the 3PEPS signal at a different temperature is shown in Figure 7. It can be seen that the peak decays slightly even at 30 K, indicating that some sort of diffusional process is still present in the polymer glass.

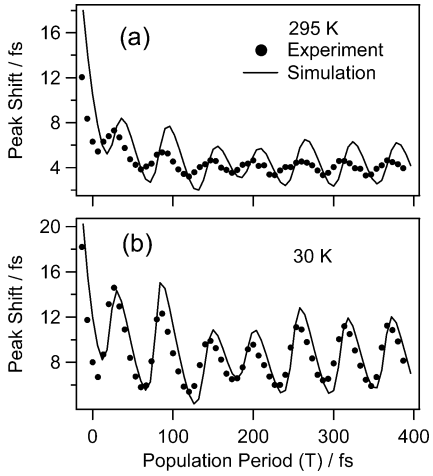

Figure 6. Experimental (filled circle) and calculated 3PEPS signal (solid curve) of NB/PMMA at (a) 295 and (b) 30 K.

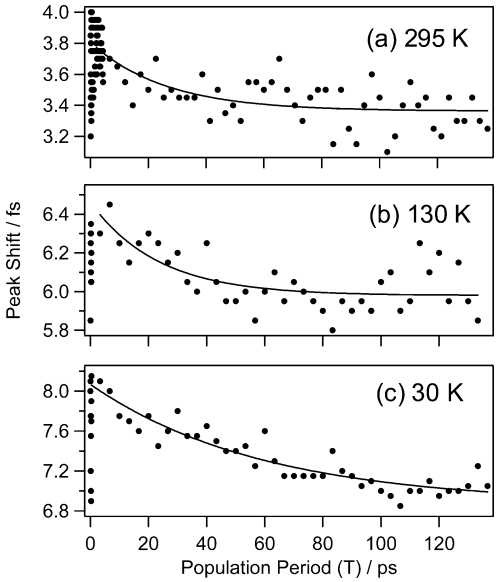

Figure 7. Picosecond portion of the 3PEPS signal of NB/PMMA at (a) 295, (b) 130, and (c) 30 K. The filled circles are the experimental results, and the solid curve is the result of fitting.

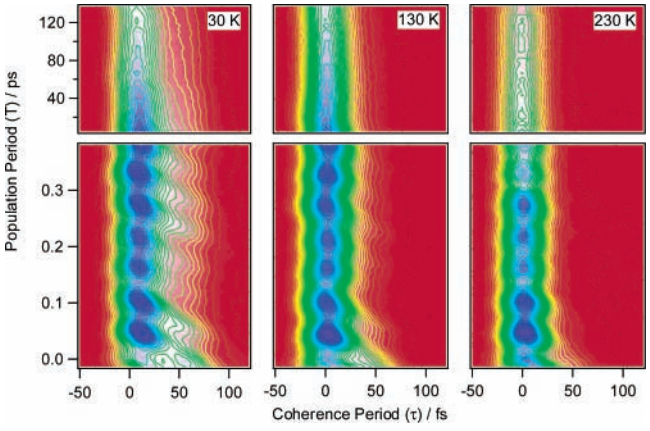

Figure 8. Temperature dependence of the two-dimensional plot of the 3PEPS-scanned photon echo signal of NB/PMMA. The temperature corresponds to 30, 130, and 230 K from left to right.

The temperature dependence of the entire 3PEPS-scanned signal is shown in Figure 8. The signal becomes thinner along the horizontal axis when the temperature is raised. The temperature dependence of the horizontal cross-section of the signal,

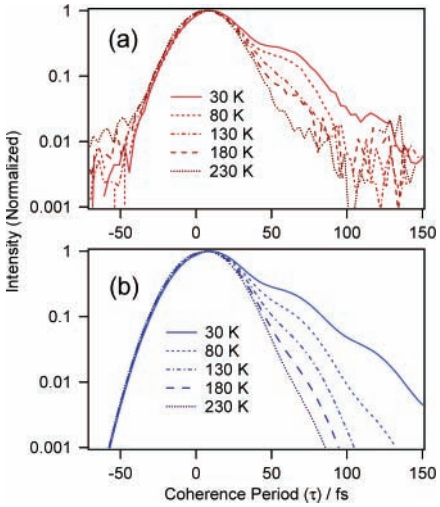

Figure 9. Temperature dependence of the (a) experimental and (b) calculated horizontal cross-section of the echo signal at $T = 387$ fs.

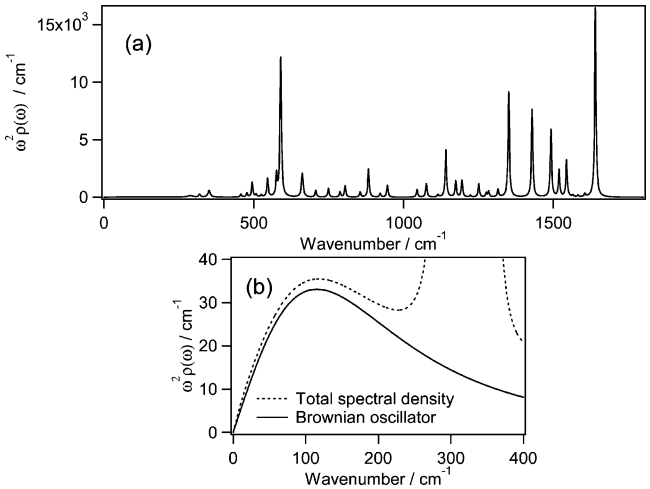

Figure 10. (a) Total spectral density of NB/PMMA used for the simulation. (b) Expansion of the low-frequency Brownian oscillator centered around 116 cm^{-1}.

which is the conventional echo signal, is shown in Figure 9a. It can be seen that the decay of the echo signal became faster at higher temperature, indicating faster optical dephasing.

4. Computer Simulations

Numerical calculations were carried out using the method developed by Mukamel[61] described elsewhere.[16,33,53] The echo signal was reconstructed starting from a model spectral density of the system. First, the line broadening function was calculated from the spectral density. Then, response functions for all of the possible double-sided Feynman diagrams were calculated from the line broadening function. Finally, the photon echo signal was constructed from a convolution of the response functions with the laser pulses, assuming a Gaussian pulse with a fwhm of 26 fs. The model spectral density we have used is shown in Figure 10. It is constructed with the intramolecular vibrational modes of NB and a phonon mode of PMMA. The frequencies of the modes were taken from the resonance Raman spectrum of NB in ethylene glycol,[62] and an exponentially damped cosine function was assumed. All of the 40 Raman active modes were included, and reorganization energies for each mode were taken from ref 26. Vibrational damping time constants were set to 2 ps, except the ones observed in the transient grating signal. Transient grating signal of NB/PMMA was measured at 9 K (Figure 1S of the Supporting Information). The damping time constants for the modes at 288, 319, 351, 495, 576, 590, and 662 cm^{-1} were 0.5, 1.6, 1.2, 2.1, 2.1, 1.9, and 1.5 ps, respectively. The damping times of the vibrational modes were not sensitive to temperature. It is known that the damping time of the mode at 590 cm^{-1} in room-temperature liquids is beyond 1.5 ps,[63,64] and a value of 2.0 ps was used in the previously reported simulation of NB in room-temperature acetonitrile.[26] Therefore, temperature dependence of the vibrational damping times was not considered in the simulation.

TABLE 1: Fitting Parameters for the Calculation of Photon Echo Signals[a]

λ_{vib}/cm^{-1}	Δ_{in}/cm^{-1}	λ_B/cm^{-1}	ω_B/cm^{-1}	γ_B/cm^{-1}
755	500	80	200	400

[a] λ_{vib}, total reorganization energy for the intramolecular vibrations of Nile blue; Δ_{in}, the inhomogeneous broadening; λ_B, reorganization energy of the Brownian oscillator; ω_B, frequency of the Brownian oscillator; and γ_B, damping constant of the Brownian oscillator. The value of λ_{vib} was taken from ref 26.

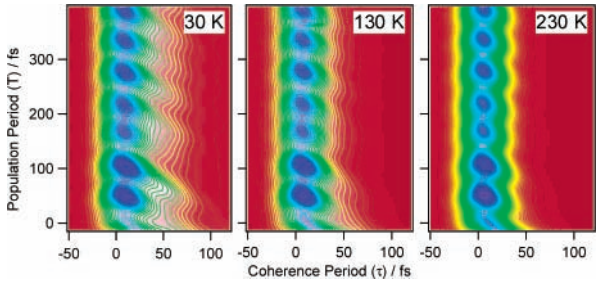

Figure 11. Calculated temperature dependence of the two-dimensional plot of the 3PEPS-scanned photon echo signal of NB/PMMA. The temperature corresponds to 30, 130, and 230 K from left to right.

The phonon mode of PMMA was approximated by a Brownian oscillator, $C(\omega)$

$$C(\omega) = \frac{2}{\pi} \frac{\lambda_B \omega_B{}^2 \omega \gamma_B}{(\omega_B{}^2 - \omega^2)^2 + \omega^2 \gamma_B{}^2} \qquad (1)$$

where λ_B, ω_B, and γ_B are the reorganization energy, frequency, and damping constant, respectively.[61] These three parameters and the inhomogeneous broadening, Δ_{in}, were the only fitting parameters. A Gaussian function, which is often used to represent the inertial component in liquids, was not used because the inertial component of PMMA is not as damped as that in liquids.[53] The fitting was carried out first to reproduce the temperature dependence of the horizontal cross-section of the echo signal shown in Figure 9, and then the entire echo signal and 3PEPS signals were fitted. The results of the fitting are shown in Table 1. The phonon mode for PMMA is shown in Figure 10b, which is a broad Brownian oscillator centered around 116 cm^{-1}. The frequency of the Brownian oscillator was taken to be $\omega_B = 200$ cm^{-1}, however the large value of $\gamma_B = 400$ cm^{-1} shifted the peak frequency to a lower value of 116 cm^{-1}. Calculated temperature dependence of 3PEPS-scanned echo signal is plotted in Figure 11, and calculated MS-scanned signal is shown in Figure 12. Both results reproduced the experimental results surprisingly well.

5. Discussion

5.1. Comparison of the Two-Dimensional 3PEPS-Scanned and MS-Scanned Signals. The 3PEPS scan and MS scan both have their own unique advantages. When the 3PEPS scan is performed, echo signals generated in the phase-matching

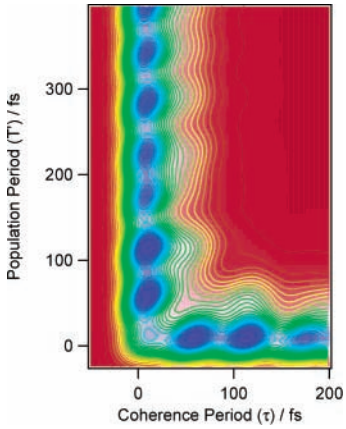

Figure 12. Calculated two-dimensional plot of MS-scanned signal of NB/PMMA at 30 K generated at the phase-matching direction of $-\mathbf{k}_1 + \mathbf{k}_2 + \mathbf{k}_3$.

direction of $-\mathbf{k}_1 + \mathbf{k}_2 + \mathbf{k}_3$ and $\mathbf{k}_1 - \mathbf{k}_2 + \mathbf{k}_3$ are time-reversals of each other. This type of measurement greatly helps to determine the exact peak shift from $\tau = 0$ fs. The peak shift can be obtained as the half of the peak to peak separation of these signals. In this manner, the accuracy of the peak shift can be as high as ± 0.3 fs.[16] The MS scan was originally applied to photon echo spectroscopy to cancel the quantum interference in the echo decay caused by coherent molecular vibrations. [19,60] In this method, the echo decay is measured in-phase with the oscillation; that is, the delay between the first and second pulses, T', is set equal to the vibrational period. The advantage of the in-phase measurement compared to out-of-phase measurement was clearly shown.[19,60] This technique was later applied to time-gated photon echo measurement.[20]

The difference between two-dimensional plot of 3PEPS-scanned and MS-scanned signals is clear by comparing Figures 3 and 4. For the 3PEPS scan, the ridge caused by the oscillation runs 45° downward, whereas that of the MS scan runs almost horizontal. For the 3PEPS scan, the only stationary pulse during each τ scan is the first pulse. When the second pulse overlaps with the first one, oscillation is caused through impulsive stimulated Raman scattering (ISRS) process and the phase of the oscillation depends on T'. When τ is increased, T' will also increase as $T' = T + \tau$. Therefore, the phase of the oscillation will be shifted forward along T when τ is increased. This is the reason the ridge caused by the oscillation runs 45° downward in 3PEPS-scanned signal. For the case of the MS scan, T' remains constant even when τ is changed. Thus, the ridge runs almost horizontal. These observations are depicted in Figure 13. The small dashed arrows represents the ridges caused by the coherent oscillation. Conventional MS-scanned echo is measured by setting the third pulse on top of one of the peaks caused by the oscillation. [19,60] When the third pulse is set in the bottom of the dip, it is the out-of-phase MS scan. For the 3PEPS scan, because the ridge runs 45° downward, the horizontal cross section will run through the ridge and cause additional modulation on the echo decay. The positions of bumps and dips caused by the ridge depend on T, and it will distort the shape of the echo decay. Therefore, the MS scan may be a better method to measure conventional echo decay.

In Figure 4, the MS-scanned signal is bent 90° near the time origin and stretches vertically and horizontally toward positive time direction. This observation can be understood when we consider the spatial configuration of the laser pulses. The signal we want to measure is the diffraction of the third pulse by the interferometric pattern created by the first and second pulses, which is generated in the phase-matching direction of $-\mathbf{k}_1 + \mathbf{k}_2 + \mathbf{k}_3$. However, in the same direction, the second pulse can be diffracted by the interferometric pattern created by the first and the third pulses. Such a misordering of the pulses happens near the time origin where the second and third pulses are not much separated. The misordered signal appears horizontally along $T' = 0$ fs toward positive τ direction in the MS-scanned signal as shown in Figure 13b. This feature was also completely reproduced by the computer simulation shown in Figure 12. For the 3PEPS scan, the misordered signal appears 45° downward as depicted in Figure 13a. Because the signal was not measured for $T < -12$ fs, the misordered signal can be hardly seen in the 3PEPS-scanned signal in Figure 3.

By careful inspection of Figure 4 one can notice that the ridge caused by the oscillation in the vertical signal along $\tau = 0$ fs is not completely horizontal. The tail of the ridge seems to be slightly slanted upward as if the phase of the oscillation is delayed with increasing τ. Similar trend can be also seen for the horizontal mis-ordered signal along $T' = 0$ fs; that is, the tail of the vertical ridge is slightly slanted to the right. Figure 14a shows the vertical cross section of the MS-scanned signal at different values of τ. It can be also seen from Figure 14a that the phase of the oscillation seems to be slightly delayed with increasing τ. For the computer simulated signal shown in Figure 14b, this trend is not as clear as the experimental one. At this point, the origin of this phase-shift is unknown, although we can speculate that it may be the effect of excited-state vibration. Prolonging the optical dephasing time by lowering the temperature may help us understand the origin of the phase-shift.

It may be interesting to mention about the relation between the two-dimensional echo signal and 3PEPS signal. In Figure 15, the peak shift is overlapped with the echo intensity counter map. It can be seen that, for the 3PEPS scan (Figure 15a), peak shift reaches its maximum just before the actual intensity peak. This is the effect of the ridge approaching from 45° downward. As the ridge approaches the peak, the peak shift will increase. Thus, the peak shift reaches its maximum right before the actual intensity peak. Peak shift of the MS-scanned signal is shown in Figure 15b. For the MS scan, only one echo signal generated at $-\mathbf{k}_1 + \mathbf{k}_2 + \mathbf{k}_3$ direction was used to obtain the peak shift; thus, its accuracy is not as high as the 3PEPS scan. However, the oscillation of the peak shift is clearly weaker than the 3PEPS scan. The ridge approaching the peak from 45 degrees downward seems to be enhancing the peak shift for the 3PEPS scan. An interesting point is that the maximum peak shift appears right after the intensity peak for the MS scan. A similar trend was also seen in the calculated signal (Figure 2s of the Supporting Information); that is, the peak shift maximum appears right before the intensity peak for the 3PEPS scan, whereas it appears right after the intensity peak for the MS scan. The intensity of the oscillation of the peak shift for the calculated MS scan was also slightly weaker than that of the calculated 3PEPS scan, although it was not as weak as the experimental one.

Comparing the experimental MS-scanned signal shown in Figure 4 and the calculated one shown in Figure 12, we have noticed another discrepancy. In the experimental signal, there is a bump caused by the oscillation along the diagonal line near $\tau = T' = 50$ fs, which is not reproduced in the calculated one (Figure 12). This discrepancy is also apparent in Figure 14. In the experimental vertical cross-section shown in Figure 14a, the second peak clearly appears around $T' = 60$ fs. However, in the calculated ones shown in Figure 14b, the second peak

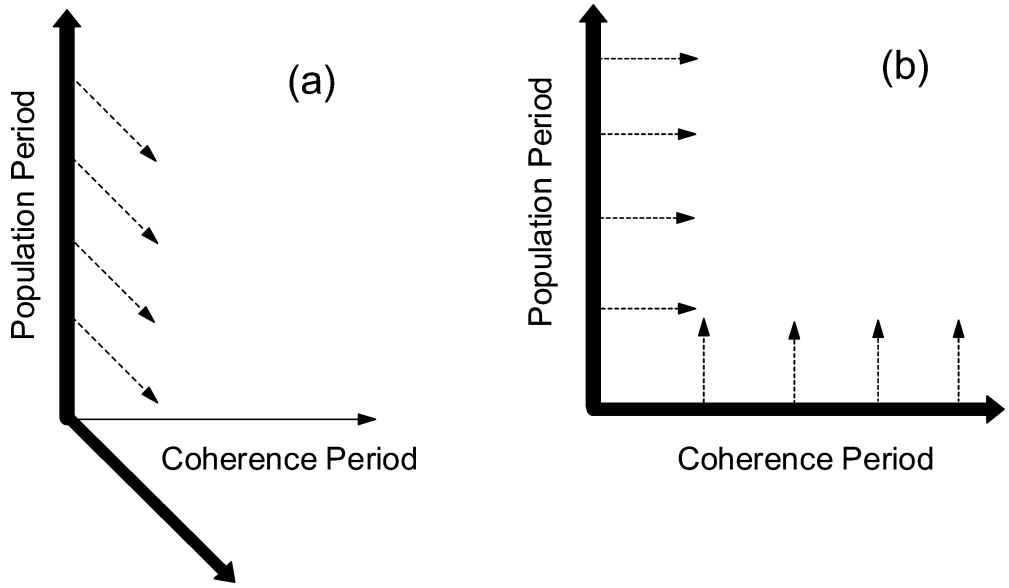

Figure 13. (a) Appearance of the echo signal for the 3PEPS scan generated in the phase-matching direction of $-\mathbf{k}_1 + \mathbf{k}_2 + \mathbf{k}_3$. The thick arrow corresponds to the position of the highest signal intensity. The dotted arrow corresponds to the direction of the ridge caused by molecular vibration. The ridge runs 45° downward. For $T < 0$ fs, the misordered signal runs 45° downward. (b) Appearance of the echo signal for the MS scan generated in the phase-matching direction of $-\mathbf{k}_1 + \mathbf{k}_2 + \mathbf{k}_3$. The misordered signal appears horizontally along $\tau = 0$ fs. The ridge caused by the oscillation runs horizontally for the normal signal, and it runs vertically for the misordered signal.

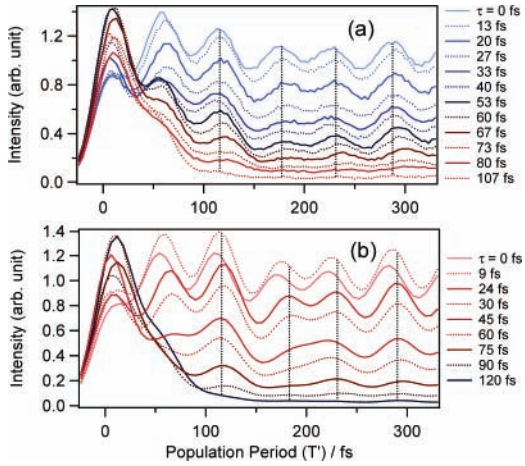

Figure 14. (a) Experimental and (b) calculated τ dependence of the vertical cross-section of the MS-scanned echo signal at 30 K.

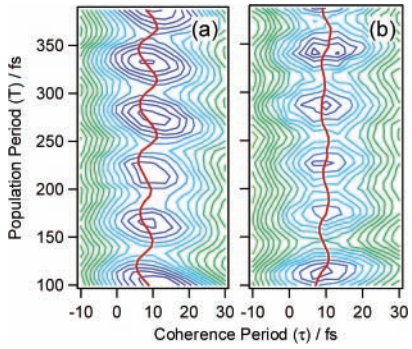

Figure 15. Comparison of the echo peak shift and intensity counter map for (a) the 3PEPS-scanned signal and (b) the MS-scanned signal at 30 K.

has weakened for $\tau \geq 45$ fs. After noticing this discrepancy, we have found that the second peak caused by the oscillation has a tendency to be stronger in the experimental results compared to the calculated ones. In Figure 5a, the second peak of the horizontal cross-section at $T = 0$ fs is stronger than the

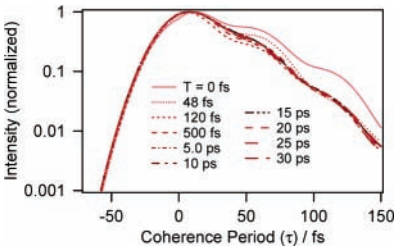

Figure 16. Calculated T dependence of the horizontal cross-section of the 3PEPS-scanned photon echo signal of NB/PMMA at 30 K generated at the phase-matching condition of $-\mathbf{k}_1 + \mathbf{k}_2 + \mathbf{k}_3$.

calculated one at $T = 0$ fs shown in Figure 16. In the experimental TG signal (Figure 3S(a) of the Supporting Information), the second peak was apparently stronger than the third peak, although the calculated one (Figure 3s(b) of the Supporting Information) was comparable to the third peak. Further investigation is necessary to specify the origin of these discrepancies.

We have compared two types of signals (the 3PEPS scan and MS scan) and examined the detailed mechanism of how the oscillation appears in 3PEPS signal. It was shown that the 3PEPS scan enhances the oscillation of the peak shift. We also found discrepancy between experimental and simulated MS-scanned signal. The diagonal bump at $\tau = T' = 50$ fs was not reproduced in the simulated signal. Several origins can be considered for this discrepancy, some unexpected interference between the signals, contribution of higher order optical nonlinear effect, anharmonicity of the phonon mode, or nonlinear coupling, and needs further investigation.

5.2. Long Time Behavior of the Echo Signal and Peak Shift. During the population period, the electronic phase information will be recorded in the interference pattern caused by the first and the second pulses. The third pulse works as a read-out-pulse, and recovery of the optical coherence leads to echo formation. Photon echo is also called the time-domain hologram and studied for application to optical memory and optical computing.[65] However, if the hologram is destroyed by some molecular motion during the population period, the

recorded memory will be lost. Thermal fluctuation of molecules above the liquid helium temperature is so intense that it has been prohibiting photon echo and hole burning to be used for the optical device. The hologram produced in the photon echo process is multidimensional in space and in frequency. Translational diffusion in glass is extremely slow. Therefore, spatial transient grating will last as long as the excited state lifetime. However, the shape of a hole burned in an absorption spectrum can be distorted in a much shorter time scale. First, the hole will become broader in the ultrafast time scale by the same molecular fluctuation causing the echo to decay. Then, it will get broader in a longer time scale by a process called spectral diffusion. This process is similar to the diffusive solvation in liquids but occurs on a much longer time scale. If the spectral interference pattern is completely destroyed by spectral diffusion and only the spatial grating pattern remains, echo formation will be prohibited and the signal will become a pure TG signal. In such a case, the signal will be symmetric reflecting the shape of the laser pulse, and two signals appearing in the two phase-matching directions will overlap at $\tau = 0$ fs without any peak shift.

It is clear from our echo signal that spectral diffusion is a minor effect in PMMA at 30 K and recovery of the coherence is still capable at $T > 100$ ps. Figure 5b shows that normalized echo signals with different T values between 30 and 130 ps overlap completely, although their total intensity decreased with increasing T, because of the decay of the excited state. An interesting point is that all those coherent oscillations observed at earlier times were not capable of erasing the phase memory. This means that the energy released by the vibrational relaxation did not seriously alter the local polymer configuration surrounding the dye molecule. Moreover, oscillation can be still seen in the echo signal at $T > 30$ ps. The vibrational damping times obtained from the oscillations in the TG signal measured at 9 K were ~2 ps or less (Figure 1S of the Supporting Information). Oscillations caused by the ISRS process should have vanished at $T > 30$ ps. Usually, vibrational lines are inhomogeneously broadened, and the homogeneous vibrational dephasing time may be much longer than the vibrational damping times obtained from TG measurement. However, it is unlikely that this fact is related to the oscillation in the τ scan at large values of T, because this is an electronic echo experiment, which is not capable of extracting homogeneous contribution out of inhomogeneously broadened vibrational line. It seems that the echo signal itself retains the oscillation caused by the first laser pulse. This means that electronic dephasing is not simply an exponential process that gives a single optical dephasing time. Similar oscillations have been observed in other photon echo experiments, although their origins have never been seriously discussed because T was set shorter than the vibrational dephasing time. We are planning to carry out heterodyne detection of the echo profile to observe how the echo signal is modulated by the oscillation. It should be interesting to see whether the oscillation appears only in the τ direction or also in the τ' direction.

Calculated T dependence of the horizontal cross-section of the echo signal is shown in Figure 16. Calculation beyond $T =$ 30 ps resulted in a distortion caused by increasing noise. This seems to be the problem of computation where the precision of the variables was limited to 15 digits. Nevertheless, it can be seen that the shape of the echo signal changed up to 500 fs indicating a fast process, whereas it did not change after 5 ps, and oscillations can be still observed up to 30 ps. The calculation also showed that the oscillation in the echo decay still exists even when T is set longer than the vibrational dephasing time. This result supports our conclusion that the echo signal itself is modulated by the vibrational coherence caused by the first pulse.

Although the shape of the echo signal did not change in the picosecond time regime, the peak shifts have decreased with increasing T as shown in Figure 7, indicating an existence of a minor spectral diffusion. The origin of this spectral diffusion could be intra- or intermolecular or both. Fitting of the peak shift in the picosecond time region resulted in a decay time constant of 59 ± 13 ps at 30 K, and the time constant shortened with increasing temperature, 23 ± 9 ps and 26 ± 7 ps at 130 and 295 K, respectively. The amplitude of the decay also decreased from 1.2 ± 0.08 fs at 30 K to 0.5 ± 0.1 fs and 0.4 ± 0.03 fs at 130 and 295 K, respectively, which were close to our experimental resolution. Decrease of the decay time constant may be due to the softening of the polymer glass by increased temperature. Decrease of the amplitude may be due to the red shift of the absorption spectrum of NB with increasing temperature. It is known that the photon echo peak shift of NB depends on excitation wavelengths.[25,26] The 3PEPS measurement was carried out for room temperature acetonitrile solution of NB at different wavelengths, and the results showed that the total peak shift value decreased when the laser wavelength was tuned to shorter wavelengths. Nevertheless, these observations suggest that the peak shift is more sensitive to spectral diffusion than the shape of the echo signal itself. Therefore, the 3PEPS measurement seems to be a sensitive technique to determine solvation dynamics in room temperature liquids. The spectral diffusion was not included in the computer simulation for two reasons: because the amplitude is extremely weak and such a slow process should not affect the ultrafast dynamics.

5.3. Temperature Dependence of the Photon Echo Signal. Temperature dependence of the photon echo signal similar to the one shown in Figure 9a was already reported by Bardeen et al.[66] The photon echo signal of a dye, LD690 (oxazine 4), was measured in PMMA and in poly(vinyl alcohol) at different temperatures between 28 and 297 K. They have observed an exponential decay and a linear temperature dependence of the decay time constant. They argued that the exponential (Markovian) decay implies that modes with frequencies greater than several hundred wavenumbers must play a role in the dephasing, whereas a linear temperature dependence of the dephasing rate implies coupling to low-frequency modes, and these two observations contradict each other. They concluded that a more complete model for optical dephasing in this temperature range is needed to explain the experimental data, possibly involving quadratic and higher order coupling terms. However, in our case, the experimental result was reproduced satisfactory by a single Brownian oscillator. Our success may be due to the broad bandwidth of this phonon mode. It extends from few tens of wavenumbers to few hundreds of wavenumbers (Figure 10b), which satisfies the requirement suggested by Bardeen et al.[66]

Although the temperature dependence of the echo decay was satisfactorily reproduced by the numerical simulation, temperature dependence of the peak shift was not so satisfactory. Peak shift at 30 K was reproduced pretty well although the one at 295 K overestimated the amplitude of the oscillation (Figure 6). Our simulation seems to have a tendency to overestimate the oscillation amplitude. The temperature dependence of TG signal, which is the vertical cross-section of the echo signal along $\tau = 0$ fs, was also measured and compared with the simulated one (Figure 3S of the Supporting Information). The amplitude of the oscillation was slightly overestimated for both temperature, 30 and 290 K. The oscillation amplitude was also overestimated for the peak shift of MS-scanned signal (Figure

2S(b) of the Supporting Information). For NB in room-temperature acetonitrile, the simulated 3PEPS signal has also overestimated the amplitude of oscillation in the experimental one. [26] Because the pulse duration was ~40 fs in this experiment, there was almost no oscillation in the experimental 3PEPS, whereas the oscillation was apparent in the simulated one. In this simulation, parameters for the intramolecular vibrations of NB were exactly the same as ours. The main origin of the oscillation is the mode at 590 cm^{-1}, which is one of the prominent modes observed in the resonance Raman spectrum of NB.[62] There is a possibility that the amplitude of this mode is overestimated. Thus, we have carried out calculations by reducing the reorganization energy of this mode from its original value of 184 cm^{-1}. However, reduction of the reorganization energy resulted in an unwanted increase of the peak shift near the time origin. It may be necessary to keep the total vibrational reorganization energy constant by increasing those of the other modes. We have also tried shifting the excitation frequency from the 0−0 transition frequency, although it resulted in the reduction of the entire peak shift but not the amplitude of the oscillation. This is consistent with the wavelength dependent 3PEPS simulations carried out for NB in acetonitrile.[26] Note that the amplitude of the picosecond decay of the 3PEPS signal shown in Figure 7 decreased with increasing temperature. This indicates that there may be a slight red shift of the absorption spectrum with increasing temperature.

5.4. Comparison with Other Photon Echo Experiments. Wavelength dependent 3PEPS measurement of NB in acetonitrile carried out by Fleming and co-workers have shown that the peak shift depends on excitation wavelength.[25,26] The entire peak shift decreased when the laser wavelength was tuned to the blue side of the absorption. It was concluded that a detailed vibronic model for the chromophore is required for a detailed quantitative analysis of the solvation dynamics of chromophores immersed in nonreacting baths. The effect of the limited "observation window" and nonlinear solvation process can also distort the 3PEPS signal. [58] Experimental conditions that favor the extraction of solvation dynamics from 3PEPS measurements include excitation on the red edge of the absorption band and the use of short, transform-limited pulses. It seems that our experiment satisfies all of these requirements; that is, detailed vibrational parameters for NB were used for the simulation, the laser frequency was set on the red side of the absorption spectrum, and the pulse duration was as short as 26 fs. The wavelength dependence is also known for conventional photon echo decay. Even at very low temperatures, the excitation of higher lying vibrations in the excited state can add a very fast component to the echo decay. [22] This can be also minimized by exciting well to the red of the inhomogeneous absorption maximum.

Fleming and co-workers also carried out temperature-dependent experiments on dyes, IR144 and DTTCI, in PMMA.[53,54] For IR144, the echo decay was almost temperature independent, and it was pulse-width-limited even at 30 K, whereas for DTTCI, it was clearly temperature dependent and the optical dephasing time became longer than the pulse duration at temperatures below 50 K. This effect was explained in terms of different coupling strength between the chromophore and the environmental fluctuation. For IR144, the reorganization energy, λ_B, of the mode peaked at ~85 cm^{-1} was estimated to be 378 cm^{-1}, whereas for DTTCI, λ_B of the mode peaked at 98 cm^{-1} was only 55 cm^{-1}. In the case of NB, λ_B of the mode peaked at 116 cm^{-1} was 80 cm^{-1}, which is rather small. Because the peak frequencies of the low-frequency modes are all similar, it should be safe to assign this mode to the phonon mode of PMMA. A similar librational mode around 100 cm^{-1} was also observed in the spontaneous nonresonant Raman spectrum[67] and in Fourier transformed spectrum of optical Kerr response of neat PMMA.[68] Inhomogeneous broadening, Δ_{in}, of NB was 500 cm^{-1}, whereas those of IR144 and DTTCI were 500 and 190 cm^{-1}, respectively. It is interesting that λ_B of NB is much smaller than that of IR144, whereas Δ_{in} of NB is comparable with that of IR144. This means that NB is less sensitive to fast environmental fluctuations, whereas its sensitivity to the slow fluctuation is comparable to that of IR144.

It can be said that optical dephasing is faster for chromophores strongly coupled to the phonon modes of the media. To slow the dephasing rate, it is necessary to choose a system with the smallest Stokes shift in a nonpolar solvent. Recently, it was shown by fluorescence anisotropy decay that the electronic dephasing time of dithiaanthracenophane in THF solution was as long as 1.0 ps at room temperature.[69] Further lengthening of the dephasing time may raise a possibility of applying photon echo technique as an optical device or to optical computing.[65]

In the wavelength dependent 3PEPS measurement of NB in acetonitrile, two solvation components was observed, i.e., a fast Gaussian component with a time constant of 130 fs which corresponds to the inertial component and a slower exponential component of 1.0 ps which corresponds to the diffusive component.[25,26] The reorganization energies for these components were 140 and 210 cm^{-1}, respectively. In the ultrafast time scale where the slower diffusive component can be approximated to be frozen, the dynamics of the liquid should be similar to the ones in glass. In that sense, a 130 fs Gaussian inertial component is equivalent to the phonon mode observed in the glass, and the diffusive component is equivalent to the inhomogeneous contribution. The reorganization energy of 210 cm^{-1} of the exponential component corresponds to a broadening of 290 cm^{-1}. From absolute resonance Raman intensity measurements of NB in ethylene glycol, it was concluded that the half-width−half-maxima of homogeneous and inhomogeneous broadenings were 350 and 313 cm^{-1}, respectively.[62] Incoherent four-wave-mixing and fluorescence-line-narrowing measurements obtained an inhomogeneous broadening of 600 cm^{-1} at fwhm in ethanol glass and in poly(vinyl alcohol).[70,71] Our simulation resulted in $\lambda_B = 80$ cm^{-1} and $\Delta_{in} = 500$ cm^{-1} which seems to be not a bad approximation.

We need to consider the origin of the phonon mode and the picosecond spectral diffusion. The origin of the phonon mode could be the hindered free rotation of the side-chains of PMMA. In room-temperature liquids, the inertial component is considered to be caused by small angle free rotations of solvent molecules in the first solvation shell surrounding the solute molecule.[1,3,5,6,9] Bardeen et al. pointed out that intramolecular motions could also contribute to the ultrafast optical dephasing because echo decays in PMMA and in poly(vinyl alcohol) were similar for LD690.[66] Because NB has a diethylamino group that can rotate and another amino group that can form intramolecular hydrogen bond, rotation of the ethyl chain or the breaking and formation of the H bond also have a possibility to contribute to the optical dephasing. Spectral diffusion can be caused by diffusive versions of such inter- and intramolecular motions or a motion of a larger portion of the polymer. Impurities such as leftover monomers and solvents may also affect such dynamics. Static inhomogeneity is caused by the frozen motion of a much larger portion of the polymer chain.

It can be said that our computer simulations reproduced the experimental observations extremely well, although there are

some mismatches between simulation and experiment. The mismatches between simulation and experiment are listed in the following.

The simulation had a tendency to overestimate the amplitude of the oscillation in (i) the room temperature 3PEPS signal (Figure 6a), (ii) the peak shift of the MS-scanned echo signal (Figure 2S of the supporting Information), and (iii) the transient grating signal (Figure 3S of the supporting Information) at both temperatures of 30 and 230 K.

The calculated 3PEPS signals gave a better fit when they were shifted 5−10 fs in the forward direction (Figure 6).

The bump appearing in the diagonal position at $\tau = T' = 50$ fs in the experimental MS-scanned signal (Figures 4 and 14a) was not reproduced in the calculated signal (Figures 12 and 14b). Similarly, the second vibrational peak appearing in the horizontal cross-section of the 3PEPS-scanned signal at $T = 0$ fs (Figure 5a), was stronger than the calculated one (Figure 16).

The phase of the oscillation seems to have gradually delayed in the experimental MS-scanned signal (Figures 4 and 14a), although such shift was not very clear in the calculated MS-scanned signal (Figures 12 and 14b).

Mismatch 3 is quite interesting, because it may be an indication of some unexpected interference between the signals. As pointed out by Bardeen et al., it may be also better to involve quadratic and higher order coupling terms to improve the reproducibility of the simulation.[66] Another method to improve reproducibility may be using an experimentally obtained response function in the frequency domain by the fluorescence-line-narrowing measurement. Such a method was applied for reproducing the incoherent degenerate-four-wave-mixing measurement, and it obtained a successful result.[66,70,71]

6. Conclusions

We have carried out a two-dimensional analysis of integrated three pulse photon echo measurement of Nile blue doped in PMMA. Vibrational relaxation was not capable of erasing the phase memory completely, and rephasing and echo formation were still clear even when the population period was extended to >100 ps. Spectral diffusion in the picosecond time scale was a minor effect, although it was detected by the 3PEPS measurement. This suggests that echo peak shift is more sensitive to slow diffusive molecular dynamics than the shape of the echo signal itself. An oscillation was present in the echo signal even when the population period was extended longer than the dephasing time of the vibrational coherence. This means that the echo signal itself is modulated by the coherent molecular vibration caused by the first pulse.

We have also carried out a computer simulation of the echo signal and it reproduced the experimental observations surprisingly well. The simulation started from a spectral density constructed from Raman active modes of Nile blue and a low-frequency Brownian oscillator. The Brownian oscillator was centered around 116 cm^{-1}, and it was assigned to the phonon mode of PMMA. The reorganization energy of the phonon mode and the inhomogeneous broadening of the NB/PMMA system were estimated to be 80 and 500 cm^{-1}, respectively.

In the future, we are planning to apply this type of method to study more complex systems which undergo a liquid−glass transition. We are also planning to carry out heterodyne detection of the echo profile in order to measure the echo signal in a three-dimensional manner. It should be interesting to observe how the echo profile is modulated by the coherent oscillation.

Acknowledgment. This research was supported by a Grant-in-Aid for Specially Promoted Research (No. 10102007) from the Ministry of Education, Science, Sports, and Culture of Japan, and the development of the Cr:F laser was partially supported by Sumitomo Foundation. Y.N. wishes to thank Prof. T. Joo for providing the original code for the 3PEPS calculation and Dr. D. Larsen, R. Jimenez, and K. Ohta for stimulating discussions.

Supporting Information Available: Figure 1S: TG signal of NB/PMMA at 9 K. Figure 2S: Comparison of the calculated echo peak shift and intensity counter map for 3PEPS-scanned and MS-scanned signals. Figure 3S: Temperature dependence of experimental and calculated TG signals. This material is available free of charge via the Internet at http://pubs.acs.org.

References and Notes

(1) Barbara, P. F.; Jarzeba, W. Ultrafast photochemical intramolecular charge and excited-state solvation. In *Advances in Photochemistry*; Voman, D. H., Hammond, G. S., Gollnick, K., Eds.; A Wiley-Interscience Publication: New York, 1990; Vol. 15, p 1.
(2) Heitele, H. *Angew. Chem., Int. Ed. Engl.* **1993**, *32*, 359.
(3) Horng, M. L.; Gardecki, J. A.; Papazyan, A.; Maroncelli, M. *J. Phys. Chem.* **1995**, *99*, 17311.
(4) Kahlow, M. A.; Jarzeba, W.; DuBruil, T. P.; Barbara, P. F. *Rev. Sci. Instrum.* **1988**, *59*, 1098.
(5) Jimenez, R.; Fleming, G. R.; Kumar, P. V.; Maroncelli, M. *Nature* **1994**, *369*, 471.
(6) Maroncelli, M. *J. Mol. Liquids* **1993**, *57*, 1.
(7) Maroncelli, M.; Flemming, G. R. *J. Chem. Phys.* **1987**, *86*, 6221.
(8) Rosenthal, S. J.; Xie, X.; Du, M.; Fleming, G. R. *J. Chem. Phys.* **1991**, *95*, 4715.
(9) Rosenthal, S. J.; Jimenez, J.; Fleming, G. R. *J. Mol. Liq.* **1994**, *60*, 25.
(10) Yoshihara, K.; Tominaga, K.; Nagasawa, Y. *Bull. Chem. Soc. Jpn.* **1995**, *68*, 697.
(11) Fourkas, J. T.; Berg, M. *J. Chem. Phys.* **1993**, *98*, 7773.
(12) Nishiyama, K.; Okada, T. *J. Phys. Chem. A* **1997**, *101*, 5729.
(13) Agarwal, R.; Prall, B. S.; Rizvi, A. H.; Yang, M.; Fleming, G. R. *J. Chem. Phys.* **2002**, *116*, 6243.
(14) de Boeij, W. P.; Pshenichnikov, M. S.; Wiersma, D. A. *Chem. Phys.* **1998**, *233*, 287.
(15) Joo, T.; Jia, Y.; Fleming, G. R. *J. Chem. Phys.* **1995**, *102*, 4063.
(16) Joo, T.; Jia, J.; Yu, J.-Y.; Lang, M. J.; Fleming, G. R. *J. Chem. Phys.* **1996**, *104*, 6089.
(17) de Boeij, W. P.; Pshenichnikov, M. S.; Wiersma, D. A. *J. Phys. Chem.* **1996**, *100*, 11806.
(18) Vöhringer, P.; Arnett, D. C.; Yang, T.-S.; Scherer, N. F. *Chem. Phys. Lett.* **1995**, *237*, 387.
(19) Bardeen, C. J.; Shank, C. V. *Chem. Phys. Lett.* **1993**, *203*, 535.
(20) de Boeij, W. P.; Pshenichnikov, M. S.; Wiersma, D. A. *J. Chem. Phys.* **1996**, *105*, 2953.
(21) Jankowiak, R.; Hayes, J. M.; Small, G. J. *Chem. Rev.* **1993**, *93*, 1471.
(22) Narasimhan, L. R.; Littau, K. A.; Pack, D. W.; Bai, Y. S.; Elschner, A.; Fayer, M. D. *Chem. Rev.* **1990**, *90*, 439.
(23) Phillips, W. A. *J. Low Temp. Phys.* **1972**, *7*, 351.
(24) Anderson, P. W.; Halperin, B. I.; Varma, C. M. *Philos. Mag.* **1972**, *25*, 1.
(25) Larsen, D. S.; Ohta, K.; Xu, Q.-H.; Cyrier, M.; Fleming, G. R. *J. Chem. Phys.* **2001**, *114*, 8008.
(26) Ohta, K.; Larsen, D. S.; Yang, M.; Fleming, G. R. *J. Chem. Phys.* **2001**, *114*, 8020.
(27) Lang, M. J.; Jordanides, X. J.; Song, X.; Fleming, G. R. *J. Chem. Phys.* **1999**, *110*, 5884.
(28) Larsen, D. S.; Ohta, K.; Fleming, G. R. *J. Chem. Phys.* **1999**, *111*, 8970.
(29) Fleming, G. R.; Cho, M. *Annu. Rev. Phys. Chem.* **1996**, *47*, 109.
(30) Passino, S. A.; Nagasawa, Y.; Joo, T.; Fleming, G. R. *J. Phys. Chem.* **1997**, *101*, 725.
(31) Passino, S. A.; Nagasawa, Y.; Fleming, G. R. *J. Chem. Phys.* **1997**, *107*, 6094.
(32) Fleming, G. R.; Passino, S. A.; Nagasawa, Y. *Philos. Trans. R. Soc. London A* **1998**, *536*, 389.
(33) Cho, M.; Yu, J.-Y.; Joo, T.; Nagasawa, Y.; Passino, S. A.; Fleming, G. R. *J. Phys. Chem.* **1996**, *100*, 11944.
(34) de Boeij, W. P.; Pshenichnikov, M. S.; Wiersma, D. A. *Chem. Phys. Lett.* **1996**, *253*, 53.

(35) de Boeij, W. P.; Pshenichnikov, M. S.; Wiersma, D. A. *Chem. Phys. Lett.* **1995**, *238*, 1.
(36) Kennis, J. T. M.; Larsen, D. S.; Ohta, K.; Facciotti, M. T.; Glaeser, R. M.; Fleming, G. R. *J. Phys. Chem. B* **2002**, *106*, 6067.
(37) Jordanides, X. J.; Lang, M. J.; Song, X.; Fleming, G. R. *J. Phys. Chem. B* **1999**, *103*, 7995.
(38) Homoelle, B. J.; Edington, M. D.; Diffey, W. M.; Beck, W. F. *J. Phys. Chem. B* **1998**, *102*, 3044.
(39) Jimenez, R.; Case, D. A.; Romesberg, F. E. *J. Phys. Chem. B* **2002**, *106*, 1090.
(40) Joo, T.; Jia, Y.; Yu, J.-Y.; Jonas, D. M.; Fleming, G. R. *J. Phys. Chem.* **1996**, *100*, 2399.
(41) Jimenez, R.; van Mourik, F.; Yu, J. Y.; Fleming, G. R. *J. Phys. Chem. B* **1997**, *101*, 7350.
(42) Yu, J.-Y.; Nagasawa, Y.; van Grondelle, R.; Fleming, G. R. *Chem. Phys. Lett.* **1997**, *280*, 404.
(43) Salverda, J. M.; van Mourik, F.; van der Zwan, G.; van Grondelle, R. *J. Phys. Chem. B* **2000**, *104*, 11395.
(44) Agarwal, R.; Krueger, B. P.; Scholes, G. D.; Yang, M.; Yom, J.; Mets, L.; Fleming, G. R. *J. Phys. Chem. B* **2000**, *104*, 2908.
(45) Agarwal, R.; Yang, M.; Xu, Q.-H.; Fleming, G. R. *J. Chem. Phys. B* **2001**, *105*, 1887.
(46) Yang, M.; Fleming, G. R. *J. Chem. Phys.* **1999**, *111*, 27.
(47) Yang, M.; Fleming, G. R. *J. Chem. Phys.* **2000**, *113*, 2823.
(48) Groot, M.-L.; Yu, J.-Y.; Agarwal, R.; Norris, J. R.; Fleming, G. R. *J. Phys. Chem. B* **1998**, *102*, 5923.
(49) Weiner, A. M.; De Silvestri, S.; Ippen, E. P. *J. Opt. Soc. Am. B* **1985**, *2*, 654.
(50) De Silvestri, S.; Weiner, A. M.; Fujimoto, J. G.; Ippen, E. P. *Chem. Phys. Lett.* **1984**, *112*, 195.
(51) Joo, T.; Albrecht, A. C. *Chem. Phys.* **1993**, *176*, 233.
(52) Nagasawa, Y.; Cho, M.; Fleming, G. R. *Faraday Discuss.* **1997**, *108*, 23.
(53) Nagasawa, Y.; Passino, S. A.; Joo, T.; Fleming, G. R. *J. Chem. Phys.* **1997**, *106*, 4840.
(54) Nagasawa, Y.; Yu, J.-Y.; Fleming, G. R. *J. Chem. Phys.* **1998**, *109*, 6175.
(55) Everitt, K. F.; Skinner, J. L. *Chem. Phys.* **2001**, *266*, 197.
(56) Bursing, H.; Ouw, D.; Kundu, S.; Vöhringer, P. *Phys. Chem. Chem. Phys.* **2001**, *3*, 2378.
(57) Xu, Q.-H.; Scholes, G. D.; Yang, M.; Fleming, G. R. *J. Phys. Chem. A* **1999**, *103*, 10348.
(58) Nagasawa, Y.; Watanabe, Y.; Takikawa, H.; Okada, T. *J. Phys. Chem. A* **2003**, *107*, 632.
(59) Nagasawa, Y.; Ando, Y.; Watanabe, A.; Okada, T. *Appl. Phys. B* **2000**, *70 [Suppl.]*, S33.
(60) Schoenlein, R. W.; Mittleman, D. M.; Shiang, J. J.; Alivisatos, A. P.; Shank, C. V. *Phys. Rev. Lett.* **1993**, *70*, 1014.
(61) Mukamel, S. *Principles of Nonlinear Optical Spectroscopy*; Oxford University Press: New York, 1995.
(62) Lawless, M. K.; Mathies, R. A. *J. Chem. Phys.* **1992**, *96*, 8037.
(63) Pollard, W. T.; Fragnito, H. L.; Bigot, J.-Y.; Shank, C. V.; Mathies, R. A. *Chem. Phys. Lett.* **1990**, *168*, 239.
(64) Fragnito, H. L.; Bigot, J.-Y.; Becker, P. C.; Shank, C. V. *Chem. Phys. Lett.* **1989**, *160*, 101.
(65) Renn, A.; Wild, U. P.; Rebane, A. *J. Phys. Chem. A* **2002**, *106*, 3045.
(66) Bardeen, C. J.; Cerullo, G.; Shank, C. V. *Chem. Phys. Lett.* **1997**, *280*, 127.
(67) Surovtsev, N. V.; Achibat, T.; Duval, E.; Mermet, A.; Novikov, N. *J. Phys.: Condens. Matter* **1995**, *7*, 8077.
(68) Kinoshita, S.; Kai, Y.; Ariyoshi, T.; Shimada, Y. *Int. J. Mod. Phys. B* **1996**, *10*, 1229.
(69) Yamazaki, I.; Akimoto, S.; Yamazaki, T.; Sato, S.; Sakata, Y. *J. Phys. Chem.* **2002**, *106*, 2122.
(70) Zhang, Y.; Hartmann, S. R.; Moshary, F. *J. Chem. Phys.* **1996**, *104*, 4380.
(71) Zhang, Y.; Hartmann, S. R.; Moshary, F. *J. Chem. Phys.* **1996**, *104*, 4371.